Nonlinear wave propagation in periodic systems: The driven sine-Gordon chain

M. D. Miller
Department of Physics, Washington State University, Pullman, Washington 99164-2814
(Received 19 August 1985)

The response of the sine-Gordon chain to an inhomogeneous dc driving force is examined. The model is discussed in terms of the nonlinear dynamics of an adsorbed monolayer solid. There are two dynamical parameters, u_p, the external driving momentum and λ, the barrier height of the substrate potential. In the adiabatic ($u_p \ll 1$, $\lambda \ll 1$) regime the dynamics is described by a propagating kink lattice with, in some cases, precursor phonons. At long times, the atoms execute periodic motion with frequencies given by harmonics of u_p. In the regime $u_p^2 \gg 2\lambda$ the system is kinetic energy dominated: There are no well-defined kinks, the wave front moves at the speed of the long-wavelength phonons, and the system is well described by the driven harmonic oscillator chain. If one increases λ at fixed u_p the motion begins to become complex and eventually one makes a transition from ordered periodic motion to disordered chaotic motion. This transition is analyzed by examination of the spectral densities of the velocity-velocity autocorrelation function, return maps, and an estimate of the maximal Lyapunov characteristic exponent. An explanation for the transition to asymptotic chaotic motion is proposed which focuses on the role of the Peierls barrier in pinning the kink lattice to the substrate. A possible application to the voltage noise spectrum in charge-density-wave materials is pointed out.

I. INTRODUCTION

The sine-Gordon (sG) equation has a long history of modeling dynamic phenomena in condensed matter systems. It appears naturally in systems which are characterized by competing length scales. Some of the better known applications of the sG equation include the Frenkel-Kontorova model of dislocation dynamics,[1] the Lee-Fukuyama model of sliding charge-density waves,[2] and the dynamics of Bloch and Néel walls.[3] In a different context, the sG equation governs the dynamics of Josephson junctions.[4] This range of applications emphasizes the need to understand the dynamics of the sG system in many different configurations.

In this paper we shall study the response of the sG chain to an inhomogeneous dc driving force. The model system which will serve as the physical analog is an impulse driven adsorbed monolayer. A semi-infinite monolayer sits in a periodic substrate potential and is subjected to a driving force on one end. The force is communicated to the lattice through the first particle (the "surface" of a semi-infinite one-dimensional structure) which acts as a "piston" driving the monolayer at constant speed. This boundary condition has been used extensively to probe nonlinear behavior (shock waves) in model lattices.[5,6]

In these model lattices, the dynamic boundary condition generates a propagating wave front with a soliton or kinklike character. At long times after the wave front has past, the system either decays to rest in the piston particle rest frame (the harmonic oscillator limit) or the particles continue to oscillate periodically (the hard rod limit). One passes from harmonic oscillator asymptotic behavior to hard rod asymptotic behavior by increasing the speed of the piston particle (or equivalently, increasing the role of the anharmonic part of the nearest-neighbor interaction). In the Toda system, the transition has been studied carefully[6] and it is found to occur at a "critical" value of the (reduced) piston particle speed.

The presence of an external field (the substrate potential) in the system studied below radically changes the nature of the long-time asymptotic behavior. In Sec. II we give the equations of motion and discuss the harmonic oscillator limit. In Sec. III we examine the propagating kink lattice and the long-time asymptotic oscillations in the adiabatic (weak-disturbance) limit. In Sec. IV, we examine the precursor phonons and obtain the lowest-order nonlinear contribution to the dispersion relation. In Sec. V, we discuss the transition to disordered (chaotic) motion treating the (magnitude of the) external field and the piston particle speed as control parameters. Section VI is the conclusion.[7]

II. EQUATIONS OF MOTION AND THE LINEAR LIMIT

As a simple model for an adsorbed monolayer, we consider N particles interacting by nearest-neighbor harmonic springs and placed in an external periodic (substrate) potential. The Lagrangian can be written

$$L = \sum_{n=0}^{\infty} \{ \tfrac{1}{2}\dot{s}_n^2 - \lambda[1-\cos(qs_n+\delta_n)] \} - \sum_{n=1}^{\infty} \tfrac{1}{2}(s_n - s_{n-1})^2 . \quad (1)$$

We introduce reduced quantities with s_n, a dimensionless displacement variable. The parameter q measures the mismatch between the monolayer and substrate. The phase δ_n is defined by

$$\delta_n = nq . \quad (2)$$

In these units, the long-wavelength speed of sound is unity. The equation of motion for the nth particle is

$$\ddot{s}_n - \Delta^2 s_n = -\lambda q \sin(q s_n + \delta_n) , \tag{3}$$

where $\Delta^2 s_n = s_{n+1} - 2s_n + s_{n-1}$ is the central second difference operator. The initial conditions, unless stated otherwise, have all particles at rest and in an equilibrium configuration

$$\ddot{s}_n(0) = \dot{s}_n(0) = 0 . \tag{4a}$$

The exception is particle 0, the piston particle, which moves at constant speed u_p at all times:

$$s_0(0) = 0, \quad \dot{s}_0(0) = u_p . \tag{4b}$$

Thus the dynamical problem is specified by assigning values to the three parameters (u_p, λ, q).

We now examine the solution to Eq. (3) in the $\lambda = 0$ (harmonic oscillator) limit. As first pointed out by Manvi, Duvall, and Lowell,[5] the exact solution for the semi-infinite linear chain with the initial and boundary conditions of Eqs. (4) can be written as

$$\ddot{s}_n = u_p (2n/t) J_{2n}(2t) \Theta(t) , \tag{5}$$

where J_{2n} is a Bessel function and $\Theta(t)$ is the Heaviside unit step function. In Fig. 1 we show s_n as a function of n for selected times between 0 and 2000. The propagation of a wave front with unit constant speed is evident [a reflection of the fact that the Bessel function in Eq. (5) is negligible until the argument is comparable to the order]. The phonon group velocity is

$$V_g = \cos\left[\frac{|k|}{2}\right] , \tag{6}$$

and thus the wave front moves at the speed of the long-wavelength phonons.

In Fig. 2, we show the velocity profile of the lattice (at $t = 1000$ and $u_p = 0.01$). In this view, the wave front shows a small overshoot, $\sim 1.2 u_p$, trailed by a fairly rapidly decaying envelope. This most important aspect of the harmonic oscillator dynamics, the relaxation of the system back to rest in the rest frame of the piston particle, is a manifestation of the dispersive nature of the excitation spectrum. An asymptotic expansion of Eq. (5) to long times yields

$$s_n \sim u_p(t-n) - \left[\frac{2}{\pi}\right]^{1/2} n u_p \frac{\cos(2t - \frac{1}{4}\pi)}{(2t)^{3/2}} , \tag{7}$$

and thus for $t/n \gg 1$, the particle moves at constant speed u_p in the lab frame. We note that the asymptotic behavior of this dynamical system differs from continuum, linear dispersive systems which decay like $t^{-1/2}$.[8] Equation (7) will play an important role in our discussion of the asymptotic behavior of the sG chain.

The piston particle does work on the rest of the chain. The power input at time t is easily shown to be

$$\frac{dE}{dt} = -u_p[s_1(t) - s_0(t)] . \tag{8}$$

At time t, the piston particle has moved a distance $u_p t$ and there are t particles behind the wave front. The mean displacement per particle behind the wave front is u_p (the lattice contraction). Therefore we obtain (the asymptotic result)

$$\frac{dE}{dt} = u_p^2 . \tag{9}$$

In Fig. 3 we show E versus t for an oscillator system with

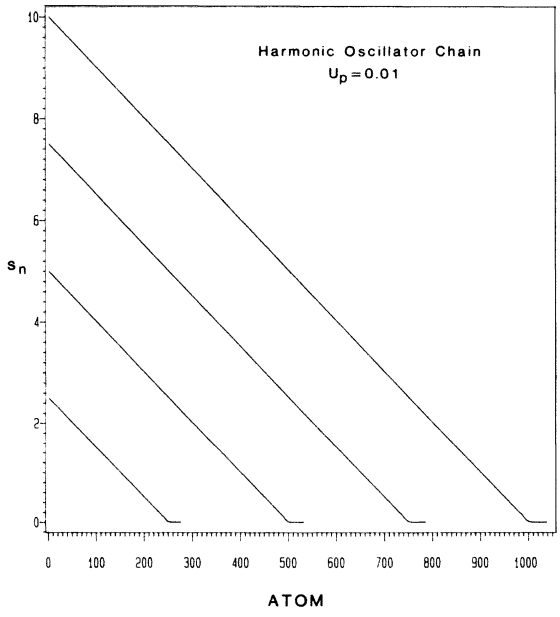

FIG. 1. Phase vs atom number for the harmonic chain with $u_p = 0.01$. The particle displacements are shown at $t = 250$, 500, 750, and 1000.

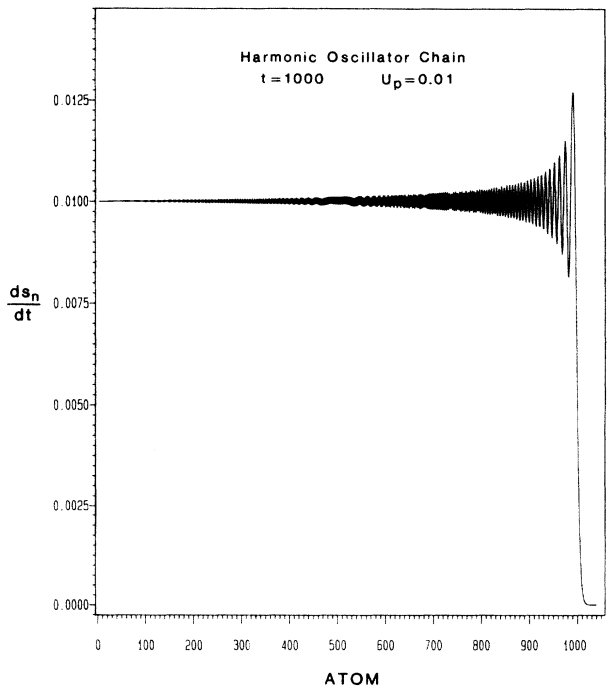

FIG. 2. Velocity profile of the harmonic oscillator chain at $t = 1000$.

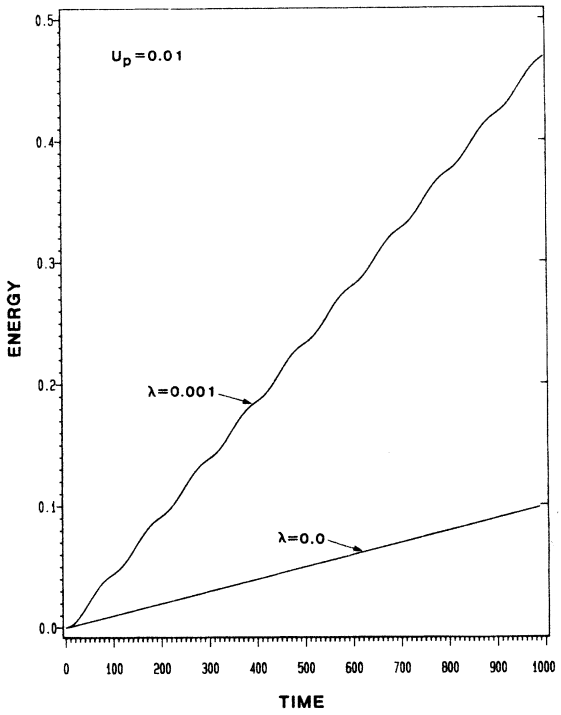

FIG. 3. Energy as a function of time for the harmonic oscillator chain ($\lambda=0.0$) and sG chain ($\lambda=0.01$) both for $u_p=0.01$. The slope of the harmonic oscillator chain (the power)$=u_p^2$, the (averaged) power for the sG chain is given by a simple soliton argument, Eq. (13).

$u_p=0.01$ and from the slope, $dE/dt=10^{-4}$, in agreement with Eq. (9).

The results of the computations reported in this section and below were obtained by stepping through the equations of motion using Verlet's procedure.[9] Thus for particle n the displacement at time step $(m+1)$ is given by

$$s_n(m+1)=2s_n(m)-s_n(m-1)+\ddot{s}_n\tau^2+O(\tau^4)\ , \quad (10)$$

where τ is the fundamental time step. (Unless otherwise indicated, all results were obtained with $\tau=0.01$.) In Table I we show a comparison between the exact, Eq. (5), and computed $\ddot{s}_n$ for $n=4$, 8, 12, 16, 20, 24, after 10000 time steps. The good agreement gives us confidence in our algorithm for at least the adiabatic (small λ, small u_p) regime.

TABLE I. Comparison of exact and calculated particle accelerations for the harmonic oscillator chain after 10000 time steps ($t=1000$, $\tau=0.01$, $u_p=0.5$).

Atom	$\ddot{s}_n$ (exact)	$\ddot{s}_n$ (calc.)	Difference (%)
0	0	0	
4	-0.256×10^{-3}	-0.263×10^{-3}	2.7
8	0.162×10^{-2}	0.161×10^{-2}	0.6
12	0.625×10^{-2}	0.624×10^{-2}	0.2
16	0.683×10^{-2}	0.685×10^{-2}	0.3
20	-0.642×10^{-2}	-0.639×10^{-2}	0.5
24	-0.956×10^{-2}	-0.959×10^{-2}	0.3

III. PROPAGATING KINK LATTICE AND ASYMPTOTIC OSCILLATIONS IN THE ADIABATIC LIMIT

In this section we switch on λ and examine the consequences on the equations of motion. The ground-state equilibrium configuration of the system is a complicated function of the parameters q and λ (the devil's staircase). In this paper we shall confine ourselves to first-order commensurate systems where $q/2\pi=1$ (i.e., the 1:1 system where the substrate and adatom periodicities are equal). For a discussion of the dynamics of the 1:2 and 2:1 systems, see Ref. 7.

In Fig. 4, we examine s_n versus atom number for the system $\lambda=0.001$ ($u_p=0.01$). The effect of the periodic external field is evident (cf. Fig. 1). The steplike propagating structure is a kink lattice. A vivid description of this process can be made by appealing to the torsion pendulum mechanical analog of the sG chain.[10] In this picture, we interpret the piston particle as winding phase on the chain at constant angular speed u_p, and the sine-Gordon soliton as the optimal way for the phase of the chain to advance 2π (i.e., from one well to the next).

There are no analytic solutions of the discrete sG equations of motion; thus, the kinklike nature of the wave front in Fig. 4 must be demonstrated. In the following, we shall identify the wave front with a kink by noting that for the parameters chosen, this system should be well approximated by the *continuum* sG chain (for which analytic solutions to the equations of motion are known) and that this analytic solution does describe the dynamics of the wave front shown in Fig. 4.

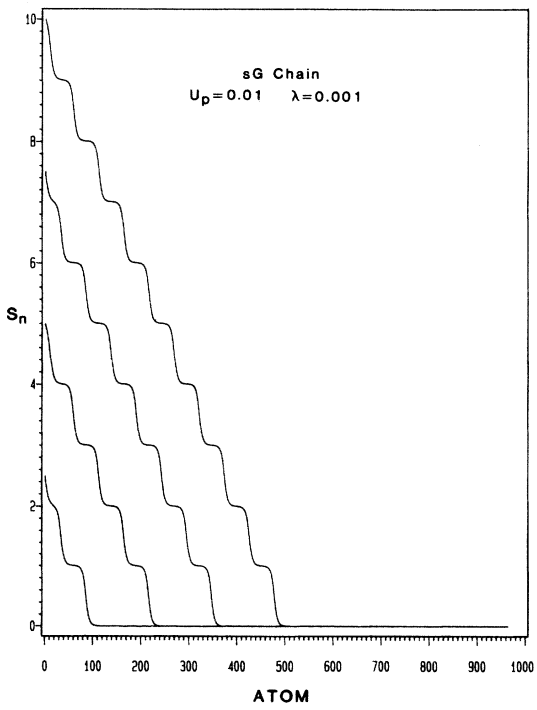

FIG. 4. Phase vs atom number for the sG chain with $u_p=0.01$ and $\lambda=0.001$. The phase profile, a propagating kink lattice, is shown at $t=250$, 500, 750, and 1000.

TABLE II. The continuum sG soliton in the reduced units of Sec. II.

Quantity	Expression
Soliton wave form	$s_s(n,t)=\frac{4}{q}\tan^{-1}[\exp(\xi_n/l_0)]$
Lorentz factor	$\gamma_s=1/(1-u_s^2)^{1/2}$
Conventional soliton size	$l_0=1/\omega_E=1/(q\lambda^{1/2})$
	$\xi_n=\gamma_s(n-u_s t)$
Particle speed on soliton wave front	$\dot{s}_s(n,t)=(2\gamma_s u_s\lambda^{1/2})\mathrm{sech}(\xi/l_0)$
Soliton energy	$E_s=8\gamma_s(\lambda^{1/2}/q)$

In Table II, we have gathered together those results of continuum sG theory which we shall need below. (A brief discussion of these results can be found in the Appendix.) We stress that the sG wave form of Table II is not a solution of the discrete sG equation of motion, Eq. (3), nevertheless in the limit $l_0 \gg 1$ it should be an excellent approximation. (For the parameters used in Fig. 4, $l_0=5$.)

The dynamics is more dramatic when viewing the velocity rather than the phase and in Fig. 5 we show the particle velocity profile at $t=1000$ for this same system. By comparing Fig. 5 with Fig. 4, we can identify the periodic array of large velocity oscillations as being the velocity pattern on the propagating kink lattice. The particle motions preceding the wave front are the precursor phonons (since from Fig. 4 it is clear that these oscillations occur in the first potential well). The precursor phonons will be discussed in detail in the next section.

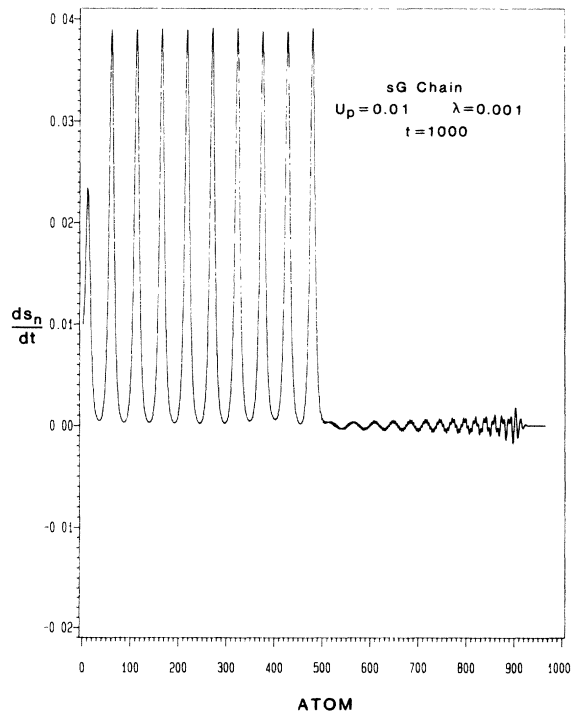

FIG. 5. Velocity profile of a sG chain with $u_p=0.01$ and $\lambda=0.001$ at $t=1000$. The periodic spikes are the particle velocity distributions on the kinks. The leading structure is the precursor phonons.

We note that the kink velocity is subsonic. Indeed, we have never found a set of parameters (including, for example, $u_p>1$) for which the wave front was supersonic. Thus some aspects of the velocity restrictions of the continuum Lorentz-invariant system persist in the discrete lattice. In this respect then there are no shock waves on the sG chain.

We compare the kinks in Fig. 5 with the continuum sG solitons. From Table II we see that the relation between the maximum particle velocity $\dot{s}_{\max}$ and the soliton velocity is given by

$$u_s=\left[1+\frac{4\lambda}{\dot{s}^2_{\max}}\right]^{-1/2}. \tag{11}$$

From Fig. 5, $\dot{s}_{\max}=0.039$, thus, $u_s=0.525$. Therefore at $t=1000$ we expect the wave front to be located approximately at atom 525. Inspection of Figs. 4 and 5 shows excellent agreement with this sG soliton-as-leading-edge picture.

We may also examine the role of solitons from the point of view of the work done on the chain by the piston particle. For a system in the adiabatic regime, most of the work done by the piston particle goes into winding kinks onto the chain. Thus if $\dot{n}_s$ is the rate of kink production, then

$$\left[\frac{dE}{dt}\right]_s=\dot{n}_s E_s\ , \tag{12}$$

where E_s is the energy per kink. For the $q=2\pi$ system of interest, $\dot{n}_s=u_p$, since in time $1/u_p$ one additional kink is formed. thus with the use of Table II we find

$$\left[\frac{dE}{dt}\right]_s=\frac{4}{\pi}\frac{u_p\lambda^{1/2}}{(1-u_s^2)^{1/2}}\ . \tag{13}$$

In Table III we compare $(dE/dt)_s$ with the calculated power for selected systems. The agreement is excellent. We also note that the exact Eq. (8) can also be used to obtain an expression such as Eq. (13). From Eq. (8) we write

$$\frac{dE}{dt}=u_p\langle\Delta s\rangle\ , \tag{14}$$

where $\langle\Delta s\rangle$ is a time averaged displacement difference along a kink. In the lab frame, a soliton consists of $\sim 4l_0/\gamma_s$ atoms ($4l_0$ is the 90-10 length of a sG soliton in its rest frame). Thus, using $l_0=1/q\lambda^{1/2}$,

$$\frac{dE}{dt}\simeq\frac{\pi}{2}\frac{u_p\lambda^{1/2}}{1-u_s^2}\ , \tag{15}$$

which agrees with Eq. (13) up to a coefficient of $O(1)$.

It is evident therefore that the wave front acts as a continuum sG soliton and that the kink dynamics is described

TABLE III. Comparison of $(dE/dt)_s$ the power input to the chain in the soliton lattice picture with $(dE/dt)_{\text{calc}}$ the calculated power input for systems with $u_p=0.01$ and varying values of λ.

λ	u_s	$(dE/dt)_s$	$(dE/dt)_{\text{calc}}$
0.001	0.53	4.7×10^{-4}	4.7×10^{-4}
0.005	0.38	9.7×10^{-4}	9.7×10^{-4}
0.010	0.33	1.4×10^{-3}	1.3×10^{-3}

excellently by the continuum wave form. Thus, understanding the dynamics of a propagating kink lattice is the key to understanding this regime. The principal function of interest is $u_s(\lambda,u_p)$. Qualitatively u_s is a monotonically decreasing function of λ and a monotonically increasing function of u_p. One can obtain an approximate relation for u_s by equating kinetic energies in the particle picture and the collective-mode (soliton) picture.

At time T the center of mass kinetic energy for the chain is

$$\kappa_p=\tfrac{1}{2}u_p^2u_sT\ , \tag{16}$$

since there are u_sT particles behind the wave front. Similarly, at time T the soliton kinetic energy is

$$\kappa_s=\frac{4}{q}\lambda^{1/2}u_s^2u_pT\ , \tag{17}$$

since there are u_pT solitons on the chain. Thus equating (16) and (17) we immediately find

$$u_s=\left[1+\frac{64\lambda}{q^2u_p^2}\right]^{-1/2}\ . \tag{18}$$

This result gives kink speeds which tend to be smaller than those measured. It is accurate in the adiabatic region, λ, $u_p\ll1$, and perhaps is exact in this limit. It gives results which are qualitatively correct for all λ and u_p! Thus, with Eq. (18), the energy per soliton E_s is given by

$$E_s=\left[u_p^2+\frac{64\lambda}{q^2}\right]^{1/2}\ , \tag{19}$$

which in the limit $\lambda=0$ reduces to the harmonic energy per particle. The comparison with the harmonic limit is simpler by considering $\varepsilon=(u_p/u_s)E_s$ the energy per particle on the kink lattice, then,

$$\varepsilon=u_p^2+\frac{64\lambda}{q^2}\ , \tag{20}$$

and the energy per particle increases linearly with λ as one moves away from the harmonic oscillator limit.

If the only motion on the chain, at long times after the passage of the wave front, were steady center-of-mass motion (as in the case of the harmonic oscillator chain) then Eq. (18) would be very accurate. However, there are also important motions of the chain in the piston particle rest frame. In Fig. 6 we show velocity as a function of time for particles 0 through 15. The particles are executing periodic motion with a period $=100$. In Fig. 7, we

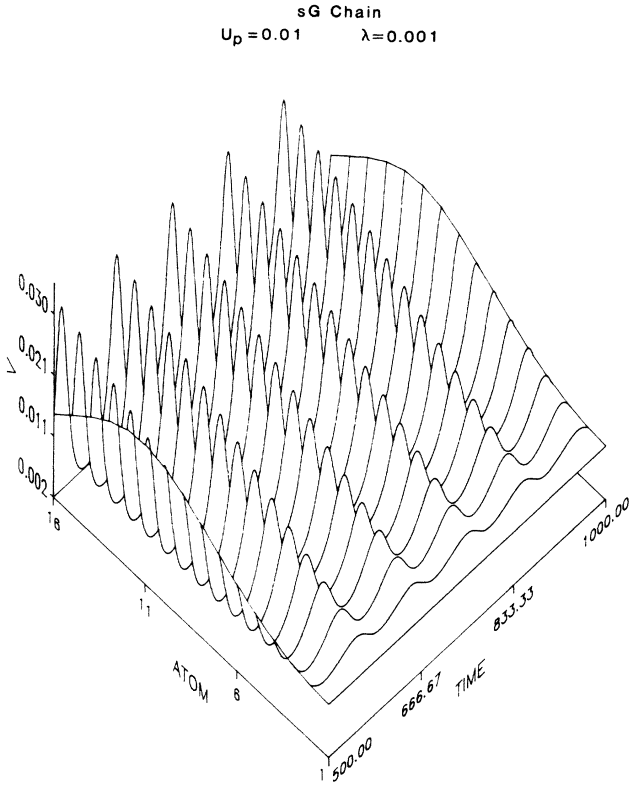

FIG. 6. Three-dimensional plot of atom velocity as a function of time for the first 16 atoms on the sG chain. The figure shows the periodic motion of each atom on the kink lattice. For this system, with $u_p=0.01$, the period $=100$.

concentrate on particle 10 and show its velocity as a function of time (in the piston particle rest frame the equivalent figure would be a closed loop from which the period could not be discerned). Asymptotically after the wave front has passed, the particle executes periodic motion with period $=100$. In order to understand these oscillations we return to the equation of motion, Eq. (3), and examine its behavior in the adiabatic limit.

If we introduce the variable $\sigma_s=qs_n$, then the equation of motion can be written as

$$\ddot{\sigma}_n-\Delta^2\sigma_n=\omega_E^2\sin(\sigma_n)\ , \tag{21}$$

where

$$\omega_E^2=\lambda q^2\ . \tag{22}$$

In the limit $\omega_E^2\ll1$, we presume that σ_n can be written in perturbative form

$$\sigma_n=\sum_{j=0}^{\infty}\omega_E^{2j}\sigma_{nj}\ . \tag{23}$$

Note that this does *not* require σ_n to be small and, in fact, from Eq. (7), $\sigma_{n0}\sim O(t)$. Then, substituting (23) into (21) and equating powers of ω_E^2 we find

$$\ddot{\sigma}_{no}-\Delta^2\sigma_{n0}=0\ , \tag{24a}$$

$$\ddot{\sigma}_{n1}-\Delta^2\sigma_{n1}=-\sin(\sigma_{n0})\ , \tag{24b}$$

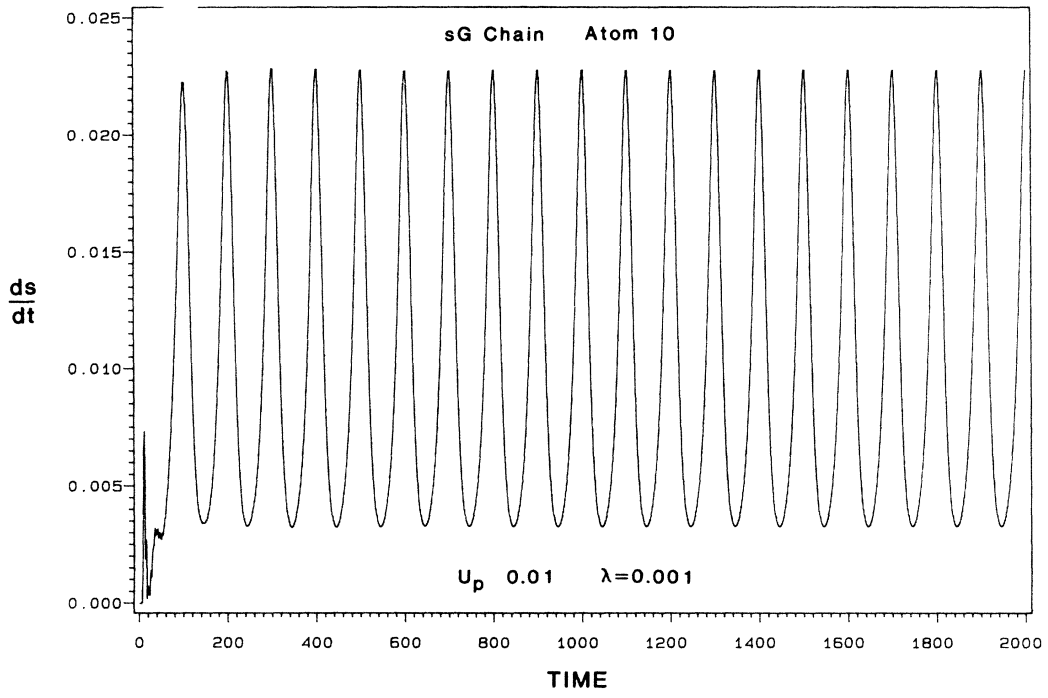

FIG. 7. Velocity as a function of time for atom 10 on the sG chain, $u_p=0.01$ and $\lambda=0.001$. This figure shows clearly the periodic velocity oscillations with period $=100$.

$$\ddot{\sigma}_{n2}-\Delta^2\sigma_{n2}=-\sigma_{n1}\cos(\sigma_{n0})\ , \tag{24c}$$

$$\ddot{\sigma}_{n3}-\Delta^2\sigma_{n3}=-[\sigma_{n2}\cos(\sigma_{n0})-\tfrac{1}{2}\sigma_{n1}^2\sin(\sigma_{n0})]\ , \tag{24d}$$

etc. In zeroth order, Eq. (24a), we have the harmonic oscillator chain whose asymptotic ($t\gg n$) behavior is determined by Eq. (7), viz.,

$$\sigma_{n0}\sim qu_pt\ . \tag{25}$$

Thus, Eq. (24b) the leading correction for finite λ behaves asymptotically like

$$\ddot{\sigma}_{n1}-\Delta^2\sigma_{n1}\approx-\sin(qu_pt)\ . \tag{26}$$

Therefore, the asymptotic dynamics of the driven sG chain (in the adiabatic regime) is determined by the ac-driven harmonic oscillator chain! The frequency of the driving force is the reduced piston particle velocity. Thus, the period is $1/u_p$ and since $u_p=0.01$, for the system of Figs. 6 and 7, the period $=100$ is now understood.

In order to more carefully assess the asymptotic periodic motion, we compute the spectral densities of the velocity-velocity or position-position autocorrelation functions. The velocity-velocity correlation function for particles i and j can be written as

$$\kappa_{ij}=\lim_{T\to\infty}\left[\frac{1}{T}\int_0^T v_i(t+t_0)v_j(t_0)dt\right]\ . \tag{27}$$

Since the velocities do not correspond to a strictly stationary process, $\kappa_{ij}(t)\neq\kappa_{ji}(-t)$, and in particular κ depends on the choice of lower limit in Eq. (27). Nevertheless at long times after the passage of the wave front, the correlation functions appear stationary (i.e., we assume we have a quasistationary process). We then introduce the spectral density from the Wiener-Khinchin theorem,[11]

$$S_{ij}(\omega)=\frac{2}{\pi}\int_0^\infty\kappa_{ij}(t)\cos(\omega t)dt\ . \tag{28}$$

In Figs. 8 and 9 we show the velocity-velocity correlation functions for particles 10 and 11 ($u_p=0.01$, $\lambda=0.001$). The autocorrelation function, Fig. 8, shows the expected period equal to 100 oscillations. The off-diagonal correlation functions, Fig. 9, show a constant phase shift between otherwise identical functions.

The important spectral density (of the autocorrelation functions) is shown in Fig. 10. The abscissa is $\omega/2\pi$ and the large peak at u_p is evident. The interesting aspect of this figure is the presence of a *second* peak at $2u_p$. The origin of this second peak can be understood from the perturbation series, Eqs. (24). In second order, Eq. (24c), the right-hand-side (rhs) is $-\sigma_{n1}\cos(\sigma_{n0})$. But asymptotically, $\sigma_{n1}\sim\sin(qu_pt)$, $\sigma_{n0}\sim qu_pt\to\sigma_{n1}\cos(\sigma_{n0})$ and thus the rhs of (24c) is $\sim\sin(q\,2u_pt)$. Indeed in the nth term of the perturbation series there appears a term like $\sin(qnu_pt)$ on the rhs. This is easily shown to be true by noting that, since Eq. (23) is a power series in λ, increasing λ at fixed u_p should generate additional peaks at higher harmonics. However, fixing λ and increasing u_p should not introduce higher harmonics. In Fig. 11, we show $S(\omega)$ for $\lambda=0.015$, $u_p=0.01$, and eight higher harmonics are clearly observable. In Fig. 12 we show $S(\omega)$ for the system $\lambda=0.001$ and $u_p=0.05$ and we see a two-

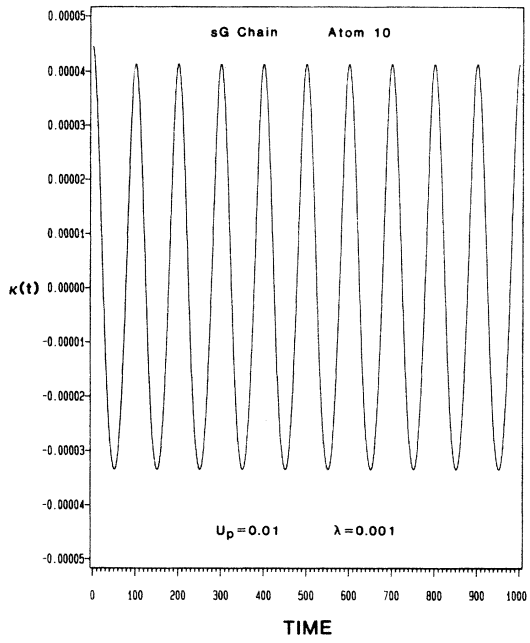

FIG. 8. Velocity-velocity autocorrelation function for the velocity history shown in Fig. 7 (atom 10, $u_p=0.01$, $\lambda=0.001$). The periodic structure with period $=100$ is evident.

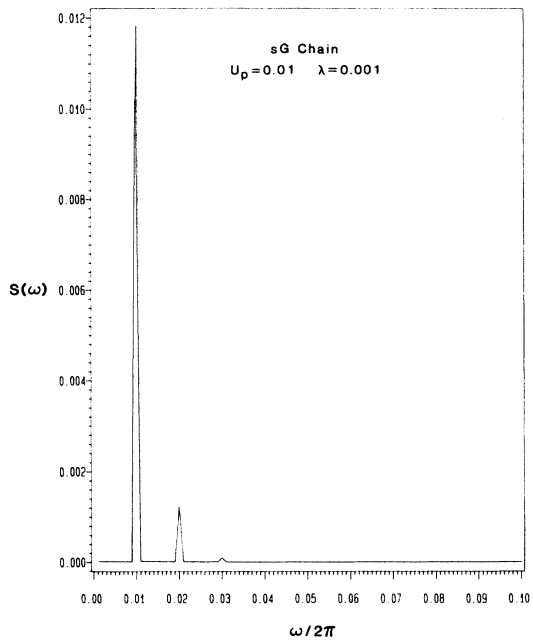

FIG. 10. Spectral density of the velocity-velocity autocorrelation function (power spectrum) of Fig. 8. This figure shows a major frequency component at $\omega/2\pi=0.01$, which is evident in Figs. 7 and 8, and also two harmonics at 0.02 and 0.03. The $\omega=0$ term has been omitted and the peaks are basically δ functions whose widths are determined by the grid spacing ($\Delta\omega=0.001$).

peak structure similar to that of Fig. 10. The physical basis for the appearance of higher harmonics can be understood from Fig. 13, the velocity autocorrelation function. This structure simply reflects the increasing tendency for particles to be found (oscillating) near the potential well minimum as λ is increased. Thus, in summary, the

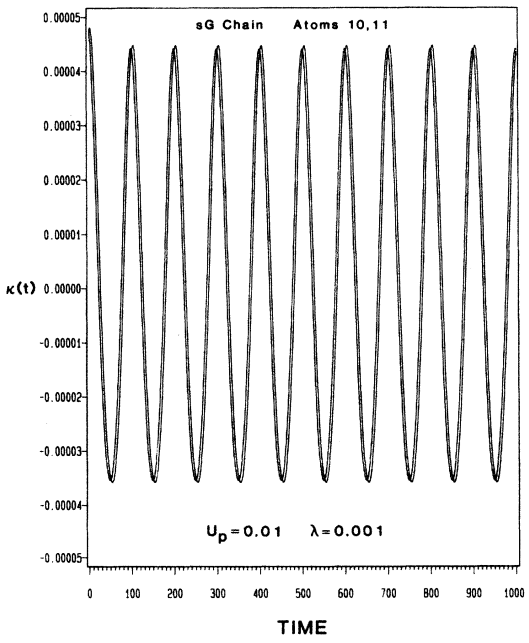

FIG. 9. The (off-diagonal) velocity-velocity correlation functions for atoms 10 and 11. Both correlation functions exhibit period $=100$ oscillations.

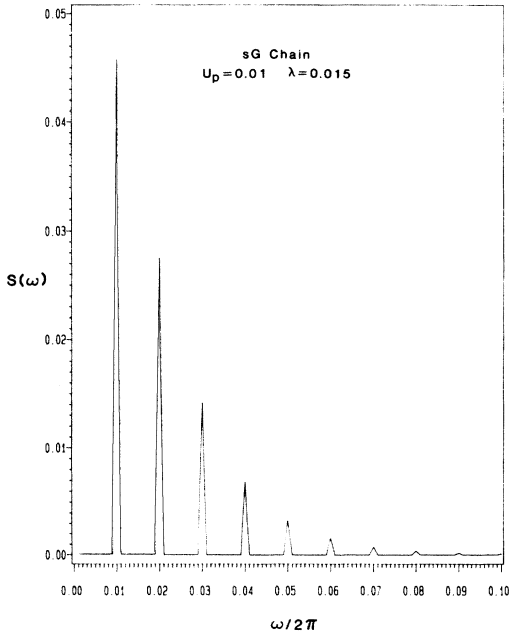

FIG. 11. Spectral density for the system $u_p=0.01$ and $\lambda=0.015$. The fundamental frequency $\omega/2\pi=u_p$ plus an additional eight harmonics are shown. There is no evidence of any other frequency components.

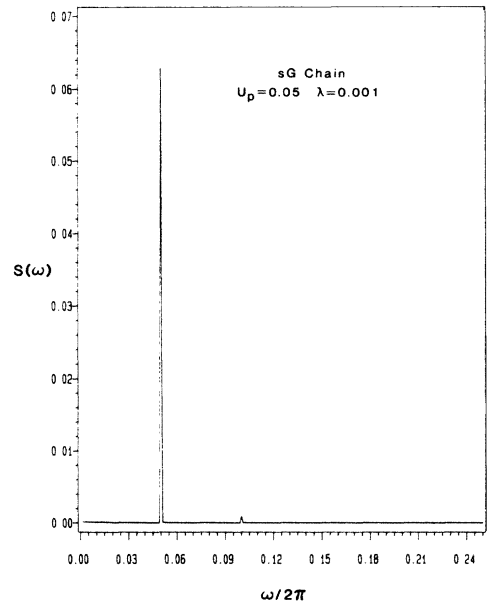

FIG. 12. Spectral density for atom 10 and the system $u_p=0.05$ and $\lambda=0.001$. This figure should be compared with Figs. 10 and 11. It demonstrates that the increased complexity in the velocity patterns come from increasing λ and not u_p.

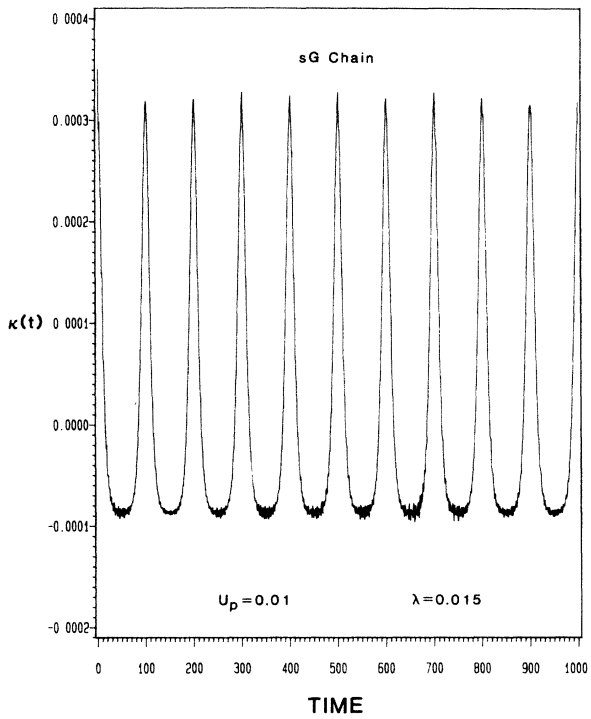

FIG. 13. Velocity-velocity autocorrelation function for atom 10 with $u_p=0.01$ and $\lambda=0.015$ whose spectral density is shown in Fig. 11.

harmonic structure seen in the velocity auto-correlation function is a function of λ the reduced barrier height.

IV. PRECURSOR PHONONS

In the preceding section, we noted, in passing, the very leading edge of the wave front as shown in Fig. 5. Reference to Fig. 4, the phase-atom plane, shows that these oscillations are localized within the first potential well and thus they can be described as phononlike excitations. Their most interesting aspect is the fact that they are moving so slowly (from Fig. 5 it is clear that the fastest phonons are moving with speed $v_{\max}\approx 0.9$).

For the atoms involved with this motion we have $s_n<1$, thus, expanding Eq. (1), the Lagrangian, in powers of s_n, this intrawell motion can be described by

$$L=\sum_n \tfrac{1}{2}\dot{s}_n^2-(s_n-s_{n-1})^2-\tfrac{1}{2}\omega_E^2 s_n^2+\frac{1}{4!}\omega_E^2 q^2 s_n^4 , \tag{29}$$

where we have included the lowest-order nonlinear contribution and $\omega_E^2=\lambda q^2$ plays the role of an Einstein frequency in the externally applied field. The nonlinear dispersion relation generated by the Lagrangian of Eq. (29) can be obtained by means of Whitham's variational approach.[12,13] This technique was first applied to lattice systems by Lowell.[14]

We search for a solution to (29) in the *form* of a uniform periodic wave:

$$s_n=\sum_{p=1}^{\infty} c_p\cos(p\theta+s_p) . \tag{30}$$

After some algebra we obtain for the average Lagrangian per particle

$$\langle L_n\rangle=\tfrac{1}{2}\sum_{p=1}^{\infty}\lambda_p c_p^2+\beta\left[\tfrac{3}{8}\sum_{\substack{p,l=1\\ m<p+l}}^{\infty} c_p c_l c_m c_{p+l-m}+\tfrac{1}{2}\sum_{p,l,m=1}^{\infty} c_p c_l c_m c_{p+l+m}\right] , \tag{31}$$

where

$$\lambda_p=\tfrac{1}{2}(\omega^2 p^2-\omega_E^2)-2\sin^2(\tfrac{1}{2}pk) , \tag{32}$$

$$\beta=\frac{1}{4!}\omega_E^2 q^2 , \tag{33}$$

and the average is defined by

$$\langle(\cdots)\rangle=\frac{1}{2\pi}\int_0^{2\pi}(\cdots)d\theta . \tag{34}$$

The averaging effectively integrates out the fast degrees of freedom (since $\theta=kn-\omega t$).

We now reorder the series in powers of β keeping only the lowest-order nonlinear contribution,

$$\langle L_n\rangle=\tfrac{1}{2}\lambda_1 c^2+\tfrac{3}{8}\beta c^4+O(\beta^2) \tag{35}$$

(where $c\equiv c_1$). The dispersion relation is given by $\partial\langle L_n\rangle/\partial c=0$ and so

$$\omega^2=\omega_E^2+4\sin^2(\tfrac{1}{2}k)-3\beta c^2 . \tag{36}$$

The amplitude function is determined by the continuity

equation $\partial k/\partial t + \partial\omega/\partial s = 0$,

$$\frac{\partial c^2}{\partial t} + \frac{\partial[c^2\cos(k/2)]}{\partial s} = 0 , \tag{37}$$

with appropriate initial and boundary conditions. [Equation (37) is identical to that obtained in linear theory.[12]]

Independent of the functional form of c, it is clear from Eq. (36) that the presence of the nonlinear term tends to *decrease* the phase and (almost certainly) the group velocities from their linear values. The basic cause of the slow phonons, however, is the first term in Eq. (36) (the gap in the spectrum) and not the nonlinear term. It is easy to show from Eq. (36) (with $\beta=0$) that for a given ω_E the maximum group velocity is given by

$$v_{\max}^2 = 1 + \tfrac{1}{2}[\omega_E^2 - \omega_E(4+\omega_E^2)^{1/2}] , \tag{38}$$

which corresponds to a wave vector $k_{\max}$ such that

$$v_{\max}^2 = \cos(k_{\max}) . \tag{39}$$

In Table IV we show $v_{\max}$ and $k_{\max}$ as a function of λ and we note that for $\lambda=10^{-3}$, $v_{\max}=0.91$, which is in excellent agreement with the results of Fig. 5. In Fig. 14, we show $v_g(k)$ for a series of values for λ and the effect of the external field is evident.

The gap in the spectrum thus has an important *dynamical* physical consequence for the driven sG chain. We note, however, that for a given $\omega_E(\lambda)$ one can always make u_p sufficiently large so that the soliton wave front travels faster than $v_{\max}$ and so there are no precursor phonons. (An example can be seen below in Fig. 22 with $\lambda=10^{-3}$ and $u_p=0.10$.)

These results are specific to commensurate systems. For incommensurate systems an acoustic mode will be present which signifies that rigid translations of the monolayer relative to the substrate cost no energy.

V. CHAOTIC REGIME

In Sec. III, we noted that as we increase λ at fixed u_p there appear an increasing number of higher harmonics in the velocity autocorrelation function. They appear as a reflection of the increased probability of finding a particle near the bottoms of the potential wells. The motion of the particles in this regime is highly ordered despite the fact that it consists of many harmonics. However, if λ is

TABLE IV. The maximum phonon group velocity $v_{\max}$ as a function of the reduced barrier height [note, $\omega_E^2=(2\pi)^2\lambda$].

λ	$k_{\max}/\pi$	$v_{\max}$
0	0	1.0
10^{-4}	0.112	0.969
10^{-3}	0.194	0.906
10^{-2}	0.319	0.734
10^{-1}	0.445	0.416
10^{0}	0.492	0.155
10^{1}	0.499	0.050
∞	0.5	0.0

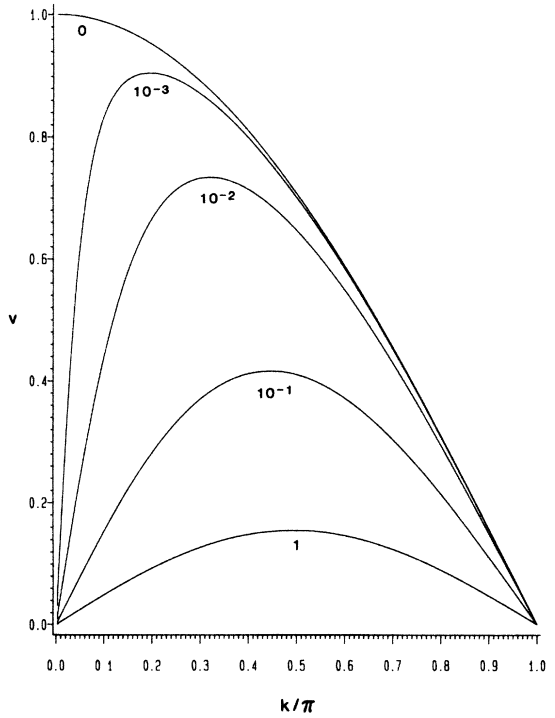

FIG. 14. Phonon group velocities as a function of k/π for commensurate monolayer systems with $\lambda=10^{-3}$, 10^{-2}, 10^{-1}, and 1. The harmonic oscillator limit is shown for comparison.

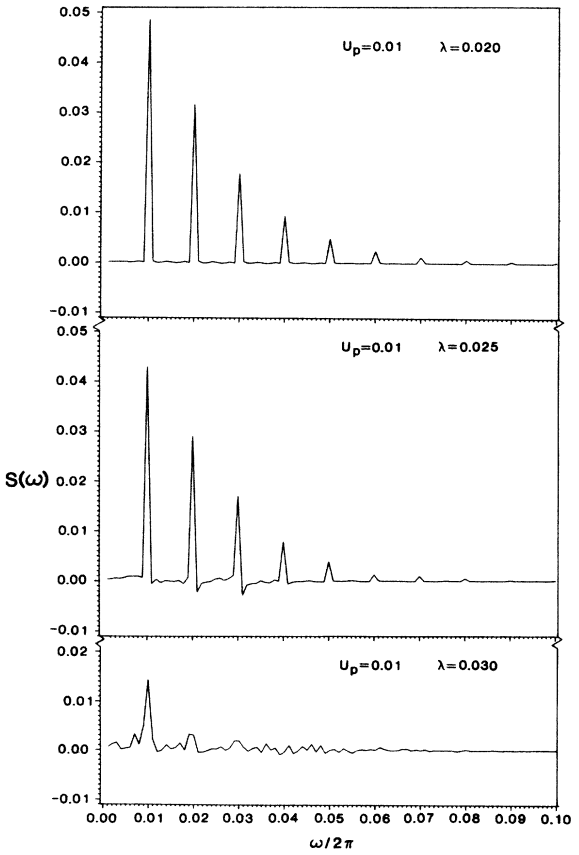

FIG. 15. Spectral densities for atom 10 and the systems $u_p=0.01$ and $\lambda=0.020$, 0.025, and 0.030. The transition from ordered to disordered behavior is evident. The peak truncation shown in the bottom figure is an artifact of the large grid size.

overly increased, the motion of the particles becomes highly disordered. In this section we discuss the transition from the ordered regime to the disordered regime.

In Fig. 15 we show $S(\omega)$ for $\lambda=0.020$, 0.025, and 0.030 ($u_p=0.01$). At $\lambda=0.020$, the spectral density begins to show structure at frequencies *other* than harmonics of u_p. The grid spacing $\Delta\omega=0.001$ is very wide and so details of the additional structure are difficult to discern, nevertheless, it does appear to have a periodic *spacing* of u_p. Increasing λ to 0.025 serves to increase the intermediate structure between the u_p harmonics. The regularity in the spacing of the intermediate structure is no longer present. By $\lambda=0.030$ it is difficult to pick out the u_p harmonics. There is apparent structure at all frequencies: the power spectrum resembles white noise. The spectra shown are for atom 10; however, they are typical of any atom on the chain.

The study of chaotic motions in dynamical systems has seen much progress in the last few years.[15] Other tools in addition to power spectra have emerged to analyze the transition from ordered to disordered behavior. We shall consider two of these: return maps and the Lyapunov characteristic numbers.

Return maps are familiar from studies of iterated maps of an interval. Circle maps[16,17] are of particular importance since they are closely related to the discretized sG equations of motion, Eqs. (3) and (10). These maps model the effects of competing frequencies and exhibit a transition to chaotic behavior. The sG equations of motions with a discretized time constitute a two-dimensional, second-order, nonlinear difference equation which can be written as

$$s_n(m+1)=2(1-\tau^2)s_n(m)+\eta_n(m)+f_n(m)\,, \qquad (40)$$

where

$$f_n(m)=-\lambda q\tau^2\sin[qs_n(m)]$$

and

$$\eta_n(m)=\tau^2[s_{n+1}(m)+s_{n-1}(m)]$$

are external "forces" acting on atom n. The coupling to the rest of the lattice, $\eta_n(m)$, appears as a noise source if the lattice is undergoing disordered motion. We shall assume that there exists a return map $g(d_n)$ such that $d_n(m+1)=g(d_n(m))$ and plot $d_n(m+1)=s_n(m+1)-s_n(m)$ as a function of $d_n(m)=s_n(m)-s_n(m-1)$. This procedure is substantiated only by the observation that the results are in complete accord with those of the power spectra. The information is complimentary to that of the power spectra in the sense that this analysis concentrates on the particle positions rather than velocities. Of course position-position correlation functions and spectral densities can be computed;[18] however, they tend to be much more featureless than the velocity correlation functions since positions are simply integrated (and thus smoothed) velocities.

In Fig. 16 we show the return map for the system $u_p=0.01$ and $\lambda=0.001$. This system, deep in the adiabatic regime, exhibits obvious periodic behavior. The time interval between points is arbitrary and for this figure was chosen to be $\Delta\tau=2$. Thus, the figure consists of 50 distinct points. As $\Delta\tau$ is decreased, the points seem to become dense on the figure. The scatter about each point is roughly a part in a thousand which is too small to be discerned on the scale of this figure.

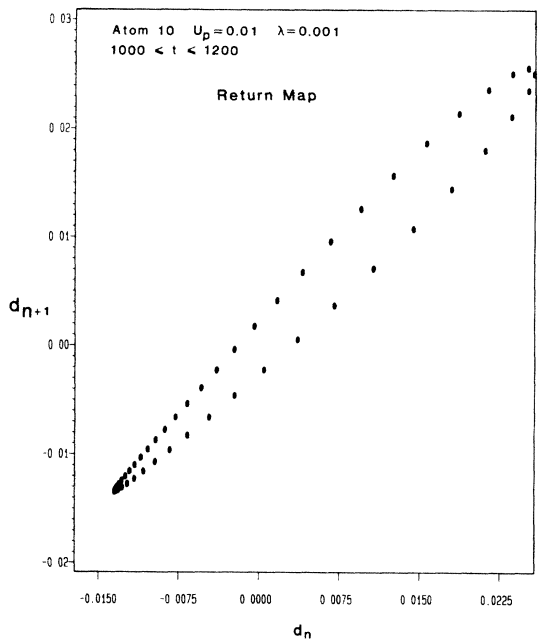

FIG. 16. Return map for atom 10 and the system $u_p=0.01$ and $\lambda=0.001$. The interval between points was chosen arbitrarily to be 2. There are 50 points representing a full cycle. This figure covers two periods and so each point was covered twice. This system is in the ordered (adiabatic) regime.

Figures 17 and 18 are for $u_p=0.01$ and $\lambda=0.015$,

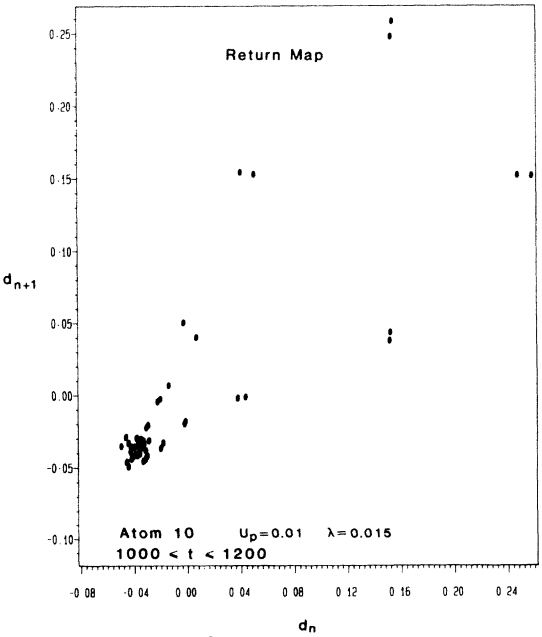

FIG. 17. Return map for atom 10 and the system $u_p=0.01$ and $\lambda=0.015$ over two periods, $1000\leq t\leq 1200$. The basic period behavior is still evident although the results for the two adjacent periods do not lie precisely on top of one another as in Fig. 16.

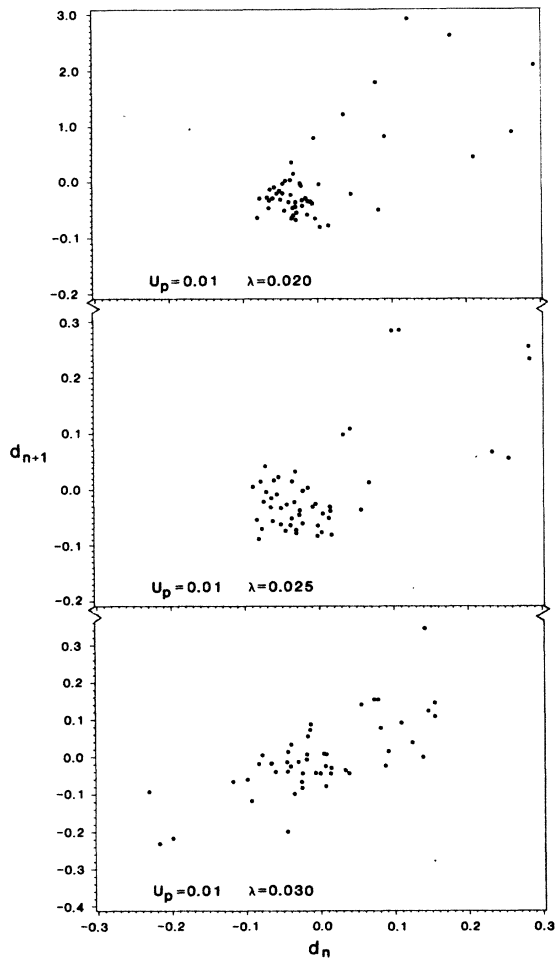

FIG. 18. Return maps for atom 10 and the systems $u_p=0.01$ and $\lambda=0.020$, 0.025, and 0.030. This figure shows the onset of disordered motion as λ is increased and should be compared with Fig. 15. The maps cover the interval $1000 \leq t \leq 1200$.

0.020, 0.025, and 0.030, respectively. (The systems whose power spectra are shown in Figs. 11 and 15, respectively.) The disorder seems to grow from the points located in the lower left corner (which represent motions in the potential well minima). Thus, in agreement with the power spectra, as λ is increased from ~ 0.015 to ~ 0.030, the motion of the particles becomes highly disordered. These return maps are in qualitative agreement with the behavior observed in studies of the circle map[19] which is important as a model for the transition to chaos in the current driven Josephson junction.[4,17,19]

Systems exhibiting chaotic motion are often described as being extremely sensitive to initial conditions.[20] A quantitative measure of this sensitivity is obtained from the maximal Lyapunov characteristic number, $\lambda_{\max}$.[21] Consider two initial configurations $\Gamma_0=\{p_0,q_0\}$ and $\Gamma_0'=\{p_0',q_0'\}$ of the N vectors of coordinates q_t and momenta p_t. We assume Γ_0 and Γ_0' are close in some sense. The equations of motion will generate a flow in phase space as a function of time and $\lambda_{\max}$ is a measure of whether the configurations Γ_t and Γ_t' stay close or diverge. Thus $\lambda_{\max}$ is obtained from

$$\lambda_{\max}=\lim_{t\to\infty}\left[\frac{1}{2t}\ln[(p_t-p_t')^2+(q_t-q_t')^2]\right]. \tag{41}$$

In order to approximate $\lambda_{\max}$ for the sG chain, we shall only consider the subset of coordinates and momenta generated by the first ten particles of the chain. The two initial configurations will be the usual equilibrium configuration, $\Gamma_0=\{s_n=0,\ \dot{s}_n=0\,|\,\forall n\}$, and a configuration identical to Γ_0 except that the *positions* of the first ten particles are chosen at random over a small interval, Δs. In Fig. 19 we show $\lambda_{\max}(t)$ for the two systems $u_p=0.01$, $\lambda=0.001$, and $u_p=0.01$, $\lambda=0.050$ (for both cases we chose $\Delta s=10^{-4}$). For the former system, we find $\lambda_{\max}<0$ for all time and thus the dynamics is stable in the sense that the long-time behavior is unaffected by a small perturbation. In the case of the $\lambda=0.050$ system, however, there are intervals of time for which $\lambda_{\max}>0$ and indeed the figure is not inconsistent with the conclusion that at long times $\lambda_{\max}$ may be positive. This certainly does not constitute proof that the system is mixing; nevertheless, its behavior is in striking contrast to the former adiabatic system. Finally we note that in this regime it is difficult to do accurate, quantitative numerical work since the time step τ must be chosen to be small relative to the smallest scale of motion in the system; however, in the chaotic regime a velocity reversal will always eventually occur in a time on the same order or smaller than τ.

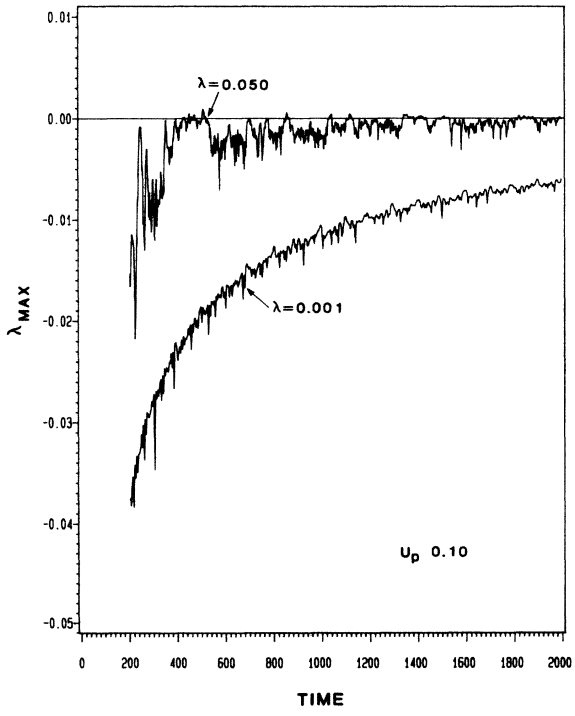

FIG. 19. The maximal Lyapunov exponents for the systems $u_p=0.01$, and $\lambda=0.001$ and 0.050.

VI. CONCLUSIONS

In this paper we have studied the response of the sG chain to an inhomogeneous dc driving force. The system has been used to model nonlinear wave propagation in an adsorbed monolayer. We have dealt mainly with systems in which the modulation of the substrate potential is small relative to the adsorbate-adsorbate interaction ($\lambda \ll 1$) and have confined the calculation to absolute zero temperature. The latter restriction is not fundamental and simply limits the results to temperatures much smaller than the Debye temperature of the solid monolayer. The Debye temperature also sets the time scale over which the piston particle impulse is applied. As an example, for a system with $T_D \approx 100$ K we have $\omega_D \approx 10^{13}$ Hz and thus an impulse lasting 10^3 oscillator cycles corresponds to an interval $\sim 10^{-10}$ sec.

In Sec. II we posed the sG dynamical problem as a function of two parameters u_p and λ (after fixing q, the static mismatch parameter). In Sec. III, we identified the region $u_p \ll 1$, $\lambda \ll 1$ as the adiabatic regime. The name is apt since in the torsion pendulum mechanical analog, the total phase difference along the chain is the extensive thermodynamic variable (conjugate to the torque) and thus for $u_p \ll 1$ the system can be compared to a box of atoms with a slowly moving wall or a pendulum whose length is slowly changing. This regime is characterized by a uniformly propagating kink lattice. The fundamental dynamical information is contained in the function $u_s(u_p,\lambda)$. A simple theory for this function yielded a result shown in Eq. (18). A striking feature of this relation is that u_s does not depend on u_p and λ separately, but only in the combination λ/u_p^2. To test this assertion in the actual system, we have plotted λ/u_p^2 as a function of u_s in Fig. 20. Also shown on this figure is Eq. (18). We conclude that the analytic result is accurate only in the limit of high kink speeds and elsewhere gives results which tend to be overly small. The λ/u_p^2 data do not fall on a universal curve; however, there is very little scatter and the worst points are in fact *not* in the adiabatic regime. One may conclude from Fig. 20 that the dominant dependence of u_s on u_p and λ is in the form λ/u_p^2.

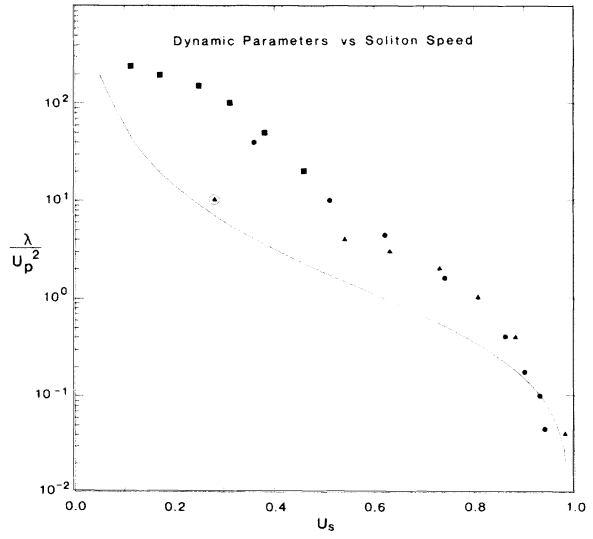

FIG. 20. λ/u_p^2 vs u_s. The ■ are data for $u_p=0.01$ and $\lambda=0.002$, 0.005, 0.010, 0.015, 0.020, and 0.025. The ● are data for $\lambda=0.001$ and $u_p=0.005$, 0.010, 0.015, 0.025, 0.050, 0.075, 0.100, and 0.150. The ▲ are data for $u_p=0.05$ and 0.0250 (the circled data point). The solid line is Eq. (18). The agreement is best in the kinetic energy dominated regime.

If either u_p or λ is made overly large, we leave the adiabatic regime. We first discuss the large u_p limit. For large u_p, the system is kinetic energy dominated and the presence of the external periodic potential becomes unimportant. That is, the piston particle simply drags the chain behind it as fast as it can go, $u_s \approx 1$, and the dynamics is described by the harmonic oscillator limit as discussed in Sec. II. Thus we expect the crossover to the kinetic energy (KE) dominated regime to occur when $\frac{1}{2}u_p^2 = 2\lambda$. This crossover is shown in Fig. 21.

One can obtain this same basic result from another point of view. In this regime, the kink speed $u_s \approx 1$ and thus using Eq. (18), we find

$$\tfrac{1}{2}u_p^2 \gg \frac{16}{q^2}2\lambda \,, \tag{42}$$

for KE domination. Further we note that in the limit $u_p \gg 1$, the kink length in the lab frame is given by

$$l_s \approx \left[\frac{32}{q^2}\right]\frac{1}{u_p} \,, \tag{43}$$

a result independent of λ.

In the vicinity of the KE dominated crossover, the velocity patterns can acquire quite complicated symmetries. For example, in Fig. 22, we show the velocity pattern for the system $\lambda=0.001$ and $u_p=0.10$ at $t=1000$. The pattern shown is periodic in time with frequency $=u_p$ and most interestingly it is also periodic as a function of atom number with a period ≈ 100.

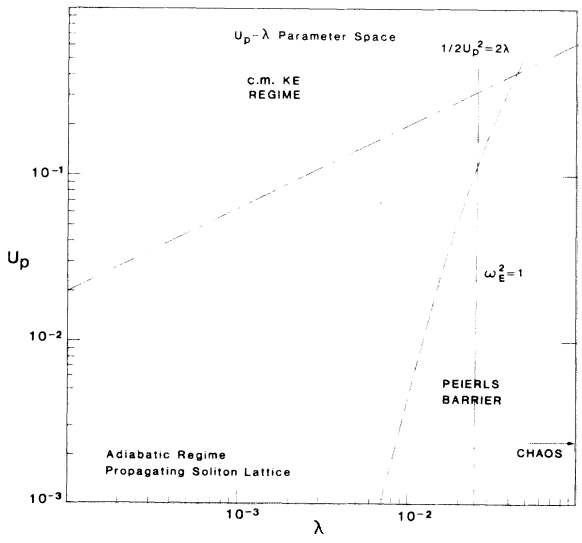

FIG. 21. u_p-λ parameter space. The short dashed vertical line is Eq. (45).

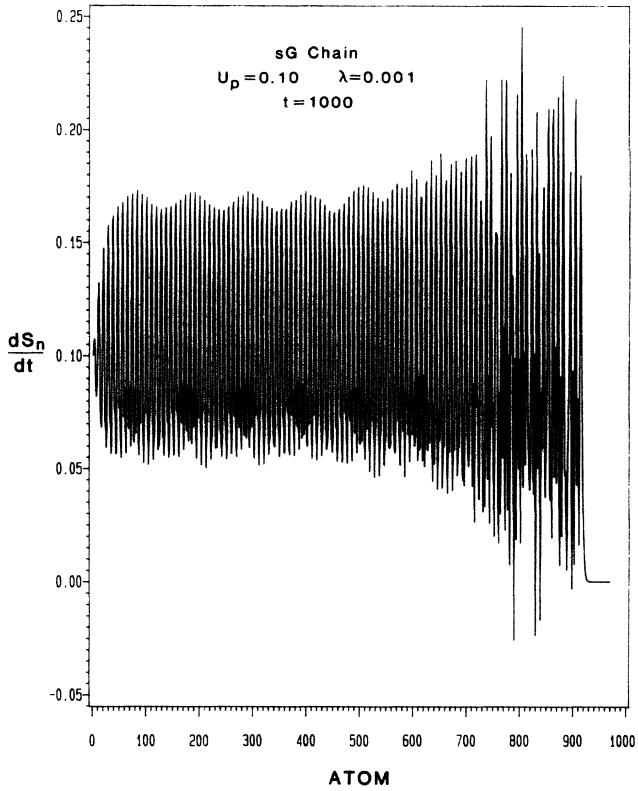

FIG. 22. Velocity profile of a sG chain with $u_p=0.10$ and $\lambda=0.001$ at $t=1000$. The pattern shown behind the wave front is periodic in time (with period 10) and periodic in atom number. The wave front is the onset of the kink lattice, there are no precursor phonons in this system.

In Sec. V, we discussed the transition to chaotic behavior when λ is increased at fixed u_p. We now wish to consider the mechanism responsible for this transition. In Sec. II, we introduced a perturbation expansion for the atom coordinates in powers of ω_E^2. For $\omega_E^2 \ll 1$ we found that perturbation theory could explain the appearance of the u_p harmonics in the particle motion. This approach should break down for $\omega_E^2 \simeq 1$ and indeed we find that this is precisely the region where the chaotic behavior begins. The conventional kink size (see Table II) $l_0=1/\omega_E$ and thus the onset of disordered behavior $l_0 \approx 1$ occurs when the kink senses the discreteness of the lattice. It is well known that, unlike in a continuum, kinks with arbitrary velocity can not propagate freely on a lattice. Kinks see a periodic potential because of the lattice symmetry and slow kinks can become pinned to the lattice. In dislocation dynamics this mechanism is well known as the Peierls barrier.[22] The Peierls barrier is the difference between a maximum energy configuration and a minimum energy configuration for a kink in a lattice. From symmetry arguments, there are only two types of extremal configurations in a uniform one-dimensional lattice. The maximum energy configuration has a kink centered on a lattice site since then a particle is on top of the potential barrier. The minimum energy configuration has the kink centered between two adjacent lattice sites. Thus, if one uses the continuum kink wave form (Table II) the Peierls barrier E_P is simple to compute numerically. (Use of the continuum wave form is justified by the discussions in Sec. III.) Indeed, with the use of the analytic continuum soliton, one can apply the Poisson summation approach of Bak and Pokrovsky[23] to derive an approximate analytic form for E_P. One finds

$$E_P=8\exp(-\pi^2 l_0)\ . \tag{44}$$

In Fig. 23 we compare Eq. (44) with the numerical results and find excellent agreement. It is apparent from Eq. (44) that the Peierls barrier is important only for small kinks. If we appeal to the collective-mode approach then a simple picture of pinning by the lattice can be obtained by setting[24]

$$\tfrac{1}{2}u_p^2=E_P(\lambda)\ . \tag{45}$$

This trajectory is shown in Fig. 21 and it clearly lies in the region where the transition from ordered to disordered motion occurs. The kink pinning can be seen vividly in Figs. 24 and 25 which show the phase s_n as a function of n for the systems $u_p=0.01$ and $\lambda=0.025$, 0.050, respectively. The nonuniform propagation of the wave fronts should be contrasted with Fig. 4.

Thus, the disordered behavior can be understood as the result of the following sequence of events. At fixed u_p, as λ is increased, the kinks slow up [Eq. (18)] and become smaller [$l_0=1/(q\lambda^{1/2})$]. At some critical value of λ [Eq. (45)] the kink motion becomes erratic due to the pinning effect of the Peierls barrier. The propagation of the wave front can be thought of as the mechanism by which the

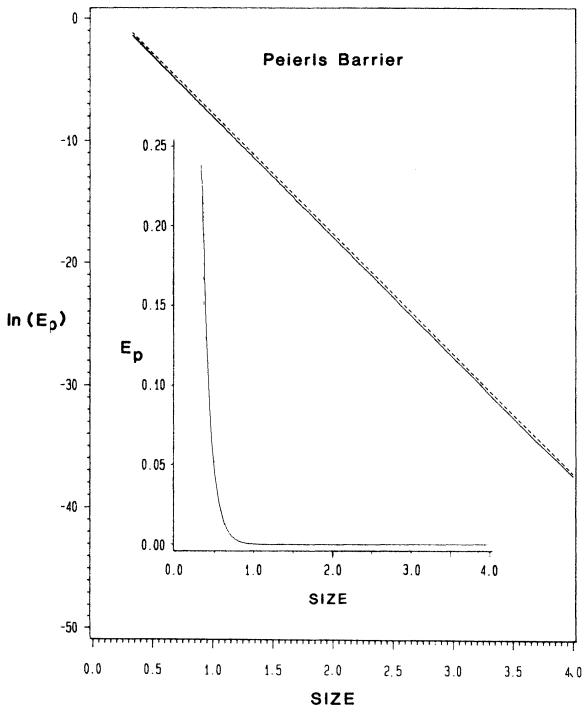

FIG. 23. $\ln(E_p)$ vs kink size l_0. The dashed line is Eq. (44) and the solid line is the numerical computation, as described in the text, and both are in excellent agreement with one another. In the inset we show E_p vs size which shows the importance of the Peierls barrier for small kinks.

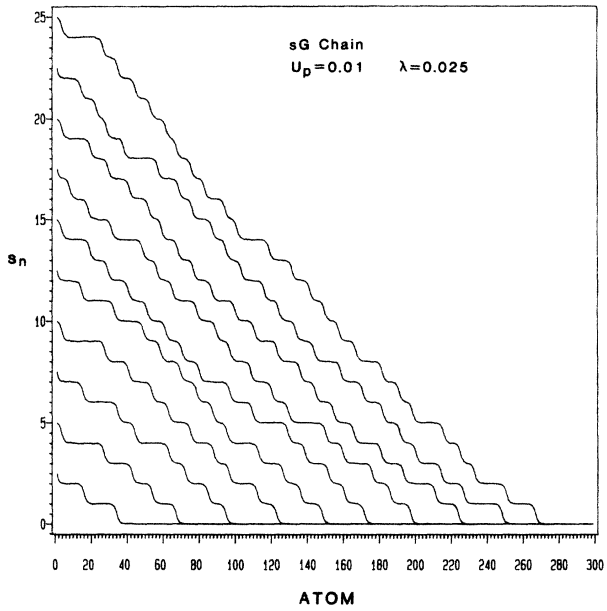

FIG. 24. Phase vs atom number for the sG chain with $u_p=0.01$ and $\lambda=0.025$. The profiles are shown for $250 \leq t \leq 2500$ in steps of 250. The time corresponding to a particular profile can easily be determined by simply referring to the position of the piston particle. The kink lattice propagates more or less uniformly until $t \approx 1500$ at which time lattice pinning of the kinks appears.

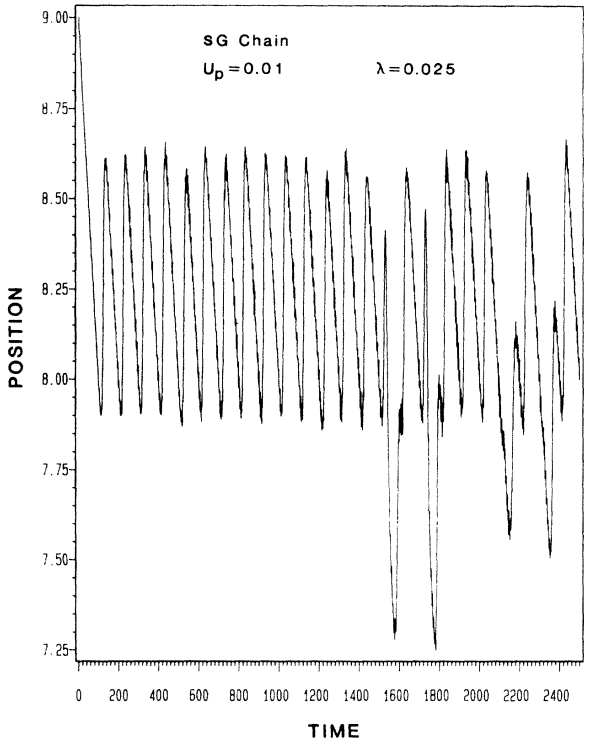

FIG. 26. The position of atom 10 (in the piston particle rest frame vs time. The atom executes ordered periodic motion until $t \approx 1500$, the onset of kink pinning (cf. Fig. 24).

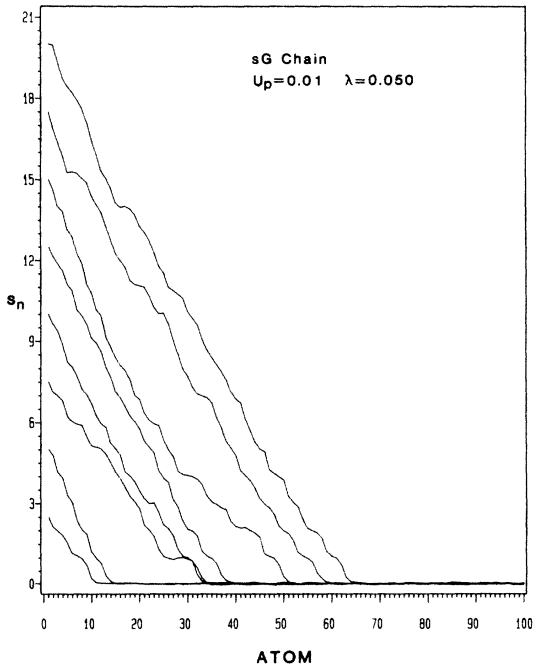

FIG. 25. Phase vs atom number for the sG chain with $u_p=0.01$ and $\lambda=0.05$. The profiles shown are for $250 \leq t \leq 2000$ in steps of 250. This system, well into the chaotic regime, shows strongly the effects of kink pinning due to the Peierls barrier.

lattice cools off a local hot spot. When the wave front is pinned over some time interval, the energy input from the piston particle is not disseminated but must be shared by the particles behind the wave front. Thus these particles are "heated up" resulting in the observed disordered motion.

This scenario can be supported by the following arguments. First, the phase plots of Fig. 24 show the wave front propagates more or less uniformly until $t \approx 1500$, when the first kink pinning occurs. In Fig. 26 we show the phase as a function of time for atom 10. The atom executes periodic motion with frequency $=0.025$ until $t \approx 1500$, *after* which the motion becomes disordered. Second, one can compute the second velocity cumulant per particle as a function of time. For systems in the adiabatic regime it goes asymptotically to some constant value. For systems in the disordered regime, the second velocity cumulant is a monotonically increasing function of time (thus, we describe the system as heating up). We note in passing that the system is not an equilibrium (Gaussian) velocity distribution since the higher cumulants do not vanish.

An implicit assumption of the above scenario (and the existence of a right-hand boundary in Fig. 21) is that there exists a critical value of λ for each u_p, below which the system will *always* execute ordered motion. We have shown this to be true numerically; however, rigorously this may not be so. The Peierls barrier never vanishes [Eq. (44) becomes exact as $l_0 \rightarrow \infty$], which leaves open the possibility that any system if followed for a sufficiently long time would begin to exhibit disordered motion and

that the "Peierls barrier" of Fig. 21 is only the crossover between systems which show disordered behavior after times $O(1)$ to systems which show disordered behavior only after exponentially long times.

The adsorbed monolayer plays a useful role as a physical model of the processes discussed in this paper but, as stressed in the Introduction, the sG equation enjoys many applications in condensed matter physics. Indeed the above results might have their most immediate application to explaining the periodic noise spectrum observed in some charge-density-wave materials. The noise voltage spectrum measured by Weger, Grüner, and Clarke[25] in $NbSe_3$ bears a striking resemblance to Fig. 11 above.

ACKNOWLEDGMENTS

Conversations with George Duvall and Sherman Lowell are gratefully acknowledged. The support of the Washington State University Computing Service Center is also gratefully acknowledged. This investigation was supported in part by funds provided by the Washington State University Research and Arts Committee.

APPENDIX: CONTINUUM LIMIT FOR THE SINE-GORDON CHAIN

In this section we very briefly describe the passage to the continuum limit and the concomitant sG soliton. The continuum Lagrangian density corresponding to Eq. (1) can be written, in physical units,

$$\mathscr{L}\left[\frac{\partial y}{\partial t},\frac{\partial y}{\partial x},y\right]=\tfrac{1}{2}\rho\left[\frac{\partial y}{\partial t}\right]^2-\frac{1}{2}T\left[\frac{\partial y}{\partial x}\right]^2-V_0[1-\cos(ky)]\ , \quad \text{(A1)}$$

where ρ is the mass density, T the tension, and V_0 the barrier height per unit length.

The equation of motion is

$$\frac{\partial^2 y}{\partial t^2}-c_0^2\frac{\partial^2 y}{\partial x^2}=-\frac{kV_0}{\rho}\sin(ky)\ , \quad \text{(A2)}$$

where $c_0^2=T/\rho$ is the longitudinal sound speed. A traveling wave solution to (A2) can be written as

$$y(\xi)=\frac{4}{k}\tan^{-1}[\exp(\xi/l_0)]\ , \quad \text{(A3)}$$

where

$$\xi=\gamma_s(x-v_s t)\ ,\qquad \gamma_s=(1-v_s^2/c_0^2)^{-1/2}\ . \quad \text{(A4)}$$

v_s is the soliton speed and from the (accidental) Lorentz invariance of Eq. (A2) it is clear that

$$v_s<c_0\ ; \quad \text{(A5)}$$

the continuum sG soliton is always *subsonic*. The conventional soliton size l_0 is given by

$$l_0=\frac{k^2 v_0}{\rho c_0^2}\ . \quad \text{(A6)}$$

The soliton energy can be easily obtained from the Hamiltonian density:

$$\mathscr{H}=\rho c_0^2\gamma_s^2[y'(\xi)]^2\ , \quad \text{(A7)}$$

and we find

$$E_s=8\rho c_0^2\gamma_s\frac{1}{k^2 l_0}\ . \quad \text{(A8)}$$

One can easily relate the particle speed to the soliton speed by use of Eq. (A3):

$$\left[\frac{\partial y}{\partial t}\right]_x=\left[\frac{2\gamma_s v_s}{k l_0}\right]\mathrm{sech}(\xi/l_0)\ . \quad \text{(A9)}$$

The entries in Table II were obtained by rewriting Eqs. (A3), (A4), and (A6)–(A8) in terms of the dimensionless units of Sec. II.

[1]A. Seeger and P. Schiller, in *Physical Acoustics,* edited by W. P. Mason (Academic, New York, 1966), Vol. III A.

[2]H. Fukuyama and P. A. Lee, Phys. Rev. B **19**, 3970 (1979).

[3]Robert M. White and Theodore H. Geballe, in *Long Range Order in Solids,* Suppl. 15 of *Solid State Physics,* edited by H. Ehrenreich, F. Seitz, and D. Turnbull (Academic, New York, 1979), Chap. VIII.

[4]D. E. McCumber, J. Appl. Phys. **39**, 3113 (1968).

[5]R. Manvi, G. E. Duvall, and S. C. Lowell, Int. J. Mech. Sci. **11**, 1 (1969); G. E. Duvall, R. Manvi, and S. C. Lowell, J. Appl. Phys. **40**, 3771 (1969); R. Manvi and G. E. Duvall, J. Phys. D **2**, 1389 (1969).

[6]B. L. Holian and G. K. Straub, Phys. Rev. B **18**, 1593 (1978); G. K. Straub, B. L. Holian, and R. G. Petschek, *ibid.* **19**, 4049 (1979); B. L. Holian, M. Flaschka, and D. W. McLaughlin, Phys. Rev. A **24**, 2595 (1981).

[7]A preliminary report of this work appeared in *Shock Waves in Condensed Matter,* edited by Y. M. Gupta (Plenum, New York, 1986).

[8]G. B. Whitham, *Linear and Nonlinear Waves* (Wiley, New York, 1974), Chap. XI.

[9]R. W. Hockney and J. W. Eastwood, *Computer Simulation Using Particles* (McGraw-Hill, New York, 1981), Chap. IV.

[10]R. A. Guyer and M. D. Miller, Phys. Rev. A **17**, 1205 (1978).

[11]N. G. van Kampen, *Stochastic Processes in Physics and Chemistry* (North-Holland, Amsterdam, 1981), pp. 60–62.

[12]G. B. Whitham, *Linear and Nonlinear Waves,* Ref. 8, Chaps. 11 and 14.

[13]A. H. Nayfeh, *Perturbation Methods* (Wiley, New York, 1973), pp. 216–222.

[14]S. C. Lowell, Proc. R. Soc. London, Ser. A **318**, 93 (1970).

[15]See, for example, the reprint collections *Universality in Chaos,* compiled by P. Cvitanović (Adam Hilger, Bristol, 1984); *Chaos,* compiled by Hao Bai-lin (World Scientific Publishing, Singapore, 1985).

[16]S. J. Shenker, Physica D **5**, 405 (1982). Reprinted in *Universality in Chaos,* Ref. 15.

[17]P. Bak, T. Bohr, M. Høgh Jensen, and P. Voetmann Christiansen, Solid State Commun. **51**, 231 (1984). M. Høgh Jensen, P. Bak, and T. Bohr, Phys. Rev. Lett. **50**, 1637 (1983).

[18]M. D. Miller (unpublished).
[19]D.-R. He, W. J. Ye, and Y. H. Kao, Phys. Rev. B **31**, 1359 (1985); P. Alstrom and M. T. Levinsen, *ibid.* **31**, 2753 (1985).
[20]R. H. G. Helleman, in *Fundamental Problems in Statistical Mechanics,* edited by E. G. D. Cohen (North-Holland, Amsterdam, 1980), Vol. 5, Sec. 2.2. Reprinted in *Universality in Chaos,* Ref. 15.
[21]B. A. Huberman and J. Rudnick, Phys. Rev. Lett. **45**, 154 (1980). Reprinted in *Universality in Chaos,* Ref. 15.
[22]R. Hobart, in *Dislocation Dynamics,* edited by A. R. Rosenfield, G. T. Hahn, A. L. Bement, Jr., and R. I. Jaffee (McGraw-Hill, New York, 1968).
[23]P. Bak and V. L. Pokrovsky, Phys. Rev. Lett. **47**, 958 (1981).
[24]J. F. Currie, S. E. Trullinger, A. R. Bishop, and J. A. Krumhansl, Phys. Rev. B **15**, 5567 (1977).
[25]M. Weger, G. Grüner, and W. G. Clarke, Solid State Commun. **44**, 1179 (1982).